

# NO Degradation on the Anatase TiO<sub>2</sub> (001) Surface in the Presence of Water

Verena Kristin Gupta,<sup>\*,†</sup> Filippo Balzaretto,<sup>‡</sup> Pu Guo,<sup>†</sup> Susan Köppen,<sup>¶,§,||</sup>

Thomas Frauenheim,<sup>\*,⊥,†</sup> and Adriel Domínguez García<sup>#</sup>

<sup>†</sup>*Bremen Center for Computational Materials Science, University of Bremen, P.O.  
Box 330440, D-28334 Bremen, Germany.*

<sup>‡</sup>*Faculty of Production Engineering, Hybrid Materials Interfaces Group (HMI), Universität  
Bremen*

<sup>¶</sup>*Hybrid Materials Interfaces Group, Faculty of Production Engineering, University of  
Bremen, Bremen, Germany*

<sup>§</sup>*Bremen Center for Computational Materials Science, University of Bremen, Bremen,  
Germany*

<sup>||</sup>*MAPEX Center for Materials and Processes, University of Bremen, Bremen, Germany*

<sup>⊥</sup>*Computational Science Research Center, No.10 East Xibeiwang Road, Beijing 100193  
and Computational Science and Applied Research Institute Shenzhen, China.*

<sup>#</sup>*Computational Science Research Center, No.10 East Xibeiwang Road, Beijing 100193  
and Computational Science and Applied Research Institute Shenzhen, China.*

E-mail: gupta@bccms.uni-bremen.de; thomas.frauenheim@bccms.uni-bremen.de

# Abstract

## Introduction

Nitrogen oxides (consisting of NO and NO<sub>2</sub>, and abbreviated as NO<sub>x</sub>) pollution is notorious for its adverse effects on human and environmental well being. NO<sub>x</sub> are produced during the process of combustion in the presence of nitrogen, e.g., in car engines and power plants [1–4]. Beyond the urge to reduce the emission of these pollutant gases, the scientific community has discussed the viability to lower their concentration in the atmosphere through their decomposition to non-hazardous compounds. NO<sub>x</sub> degradation via titania (TiO<sub>2</sub>) photocatalysis remains as a popular proposition to deal with this environmental threat. Research in this direction has been extensive [5–9]. Some investigations focus on NO<sub>x</sub> photoreactions on different crystalline modifications of titania or on commercially available TiO<sub>2</sub> powders, including studies on the effect of doping on the degradation rate of the contaminant. All these works report several reaction byproducts of the NO<sub>x</sub> photodegradation under ultraviolet (UV) irradiation.

Moreover, Freitag et al. [6] have observed the elimination of NO even under visible light conditions. The prospect of using visible light for the decomposition of NO is of great interest as it would entail a significant improvement in efficiency, considering that the visible range is about 43% of sunlight, while the UV range comprises only 2-3%. In Ref. [6], a visible light-assisted charge transfer (CT) mechanism between nitric oxide (NO) and TiO<sub>2</sub> was suggested. In this mechanism, an electron is excited from the in-gap molecular levels to the bottom of the conduction band (CB) of titania, thus leading to formation of NO<sup>+</sup> ions, which in the presence of water, may lead to formation of nitric acid (HNO<sub>3</sub>). This degradation process is intrinsically different from that commonly considered, in which electron-hole pairs are created when UV light is shone. The electrons then get trapped at surface hydroxyl groups leading to formation of hydroxide ions (OH<sup>-</sup>), which in turn react with NO to form HNO<sub>2</sub> in a first step, and HNO<sub>3</sub> finally. This NO<sub>x</sub> degradation mechanism under UV light

has been the primary focus of most investigations so far [5, 8–10], while further research is needed on the vis light activation described by Freitag and coworkers.

An important missing aspect in the aforementioned investigation is an in-depth discussion on the possible role that water and surface OH groups may play on both the adsorption and decontamination of NO on TiO<sub>2</sub>. Although the authors claim that the presence of water is essential for the degradation of the contaminant, no research has been conducted so far that address in detail how water could possibly change, if any, the conclusions drawn in that work. For example, the visible range bands observed in the absorption spectra of NO-TiO<sub>2</sub>, and key aspect for the vis light activation of the complex, might be affected when water and NO molecules compete to coadsorb on a same or neighbour surface binding sites. Furthermore, a detailed study of the possible reaction pathways leading to formation of HNO<sub>3</sub> is also called for.

In this work, we set out to explore the activation and degradation mechanisms of different NO-H<sub>2</sub>O-TiO<sub>2</sub> complexes. We study the optical absorption properties of the NO-H<sub>2</sub>O coadsorption and discuss the viability of a CT complexation in the presence of water. For this, we employ the time-dependent density functional based tight binding (TD-DFTB) method [11], which is an efficient approach for the computation of excited state properties, and especially useful for the study of large systems. Additionally, we use real-time excited state electron dynamics for a complementary analysis of the excitation process. Our results indicate the formation of negative charge carriers in the TiO<sub>2</sub> surface and positive-charged NO adsorbates, suggesting the occurrence of a CT mechanism under the effect of water. We focus on two possible reaction pathways for the decontamination of the air pollutant. Reaction barriers were calculated using first-principle ground state simulations (in dark conditions) in order to confirm, or disprove, the role of vis light activation on the degradation of NO. To simulate the excited state conditions, we model the reaction pathways using NO<sup>+</sup>. Our findings suggest that, under visible range illumination, NO may react with adsorbed OH groups

(resulting from water dissociation) to form  $\text{HNO}_2$ . Furthermore, as a competing mechanism,  $\text{NO}_2$  could be also formed on the surface via the interaction of  $\text{NO}^+$  with monocoordinated O sites, which may be observed under certain conditions.

## Methods

The anatase (001) surface was modeled using a supercell containing a slab of  $\text{TiO}_2$  and a vacuum region sufficiently large ( $\sim 20\text{\AA}$ ) to avoid spurious interaction of the surface with its periodic images. We employ the lattice constants  $a = 3.81\text{\AA}$  and  $c = 9.57\text{\AA}$ , calculated at the GGA (PBE) level of theory [12]. We consider  $4\times 4$  surface unit cells and a 8-layer slab in our model. Thus, our supercell contains altogether 384 atoms (see Fig. ??). All atoms in our system are allowed to relax. To study the (co-)adsorption of the involved molecules on the surface, adsorbents were added on each side of the slab symmetrically. Adsorption energies were calculated for several geometries in order to find the most stable atomic configurations. Additionally, we use molecular dynamic simulations to test the stability of the systems when heated up to 300 K. We obtained two non-equivalent stable co-adsorption geometries, displayed in Figure (1).

Table 1: Adsorbent ( $\text{H}_2\text{O}$  and  $\text{NO}$ ) coverages of the  $4 \times 4$  surface unit cell for the HONO and NO structural configurations. The integer value gives the total number of molecules per supercell surface. The percentage is given as adsorbents per Ti binding sites.

	$\text{H}_2\text{O}$	$\text{NO}$
$\text{NO}_{\text{OH}}$	3 (18.75%)	1 (6.25%)
$\text{NO}_{\text{Ti}}$	2 (12.5%)	1 (6.25%)

Adsorption geometries were first obtained for  $\text{H}_2\text{O}$  in different concentrations as specified in Tab. 1. Subsequently  $\text{NO}$  was added to obtain initial configurations for  $\text{NO}$  adsorbed on a hydroxyl group (in the table named  $\text{NO}_{\text{OH}}$ ) and  $\text{NO}$  adsorbed on a Titania site (named  $\text{NO}_{\text{Ti}}$ ). The configuration  $\text{NO}_{\text{Ti}}$  is equivalent to the most stable adsorption configuration of

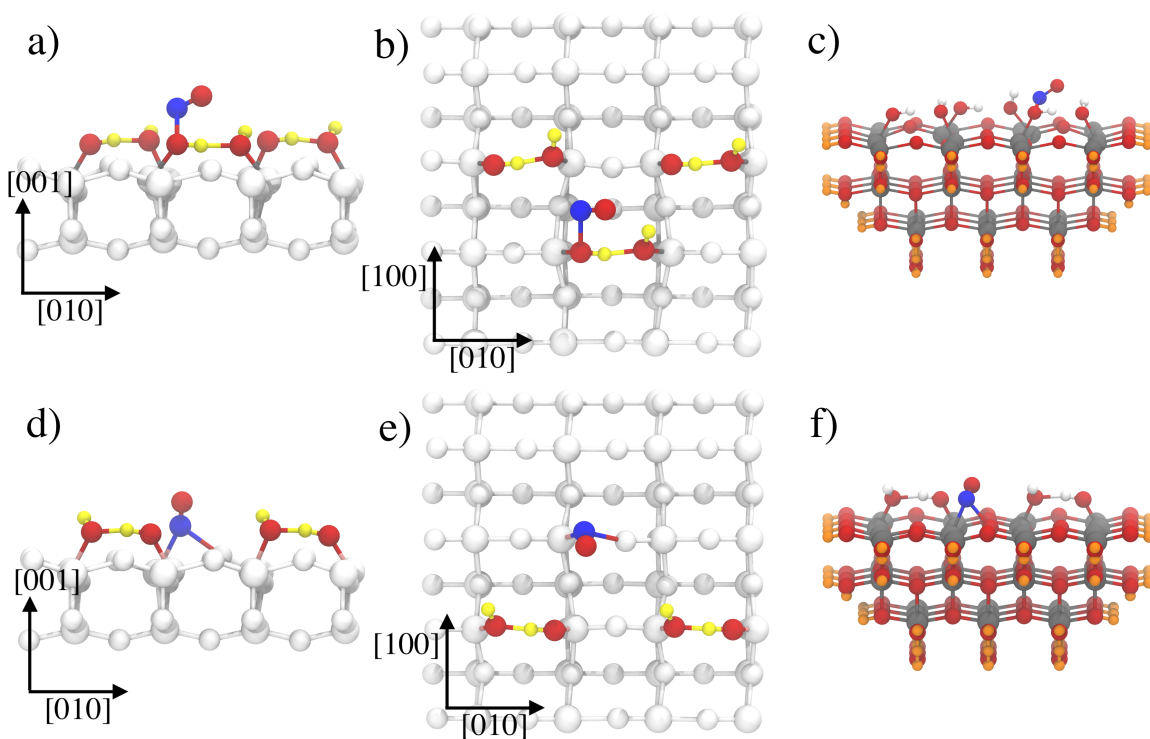


Figure 1: Adsorption structure of NO adsorbing on a bridging hydroxyl group in the sideview (a) and topview (b). Nitrogen is indicated in blue, hydrogen in yellow, oxygen in red. The slab is blended out from the adsorption geometries by displaying it in white. The same is illustrated for NO adsorbing on a five fold coordinated titanium atom in the sideview (d) and topview (e). Anatase cluster structures as used for the TD-DFTB calculations are displayed in (c) and (f). For those hydrogen is displayed in white, titanium in grey, oxygen in red and the pseudo hydrogen species ( $H'$ ) are displayed in orange. Image c) displays the cluster, called HONO-c, with  $\text{NO}+3\text{H}_2\text{O}+\text{Ti}_{37}\text{O}_{104}\text{H}'_{86}$  and f) NO (NO-c) with  $(\text{NO}+2\text{H}_2\text{O}+\text{Ti}_{37}\text{O}_{104}\text{H}'_{86})$ .

NO without water. As it turns out, different reactions occur for the two employed water coverages. For water coverages of 18.75% and greater, HONO is formed by the formation of a bond between an ionized  $\text{NO}^+$  and a Hydroxyl group, whereas for smaller coverages, NO adsorbs on the surface without direct interaction with the water molecules.

All PBE calculations, including the computation of reaction barriers to evaluate possible reactions in the dark, were performed using the Vienna ab Initio Simulation Package (VASP 5.4)[13], applying the Projector Augmented Wave (PAW) method [14] and using a cutoff energy of 700 eV for the basis set. A  $10^{-4}$  eV convergence criterion was used in the self-consistent field (SCF) calculation of the electronic energy, and the geometry optimization was terminated when the energy difference has become less than  $10^{-3}$  eV between two steps. We employed a  $2 \times 2 \times 1$  Monkhorst-Pack [15] k-point grid to sample the Brillouin zone (BZ). Reaction barriers were calculated via the nudged elastic band (NEB) method as implemented in the VTST-tools package [16, 17]. The climbing image method was used with 7 to 15 images, depending on the system. The saddle point was subsequently determined using the DIMER method [18, 19].

To study the system after excitation, we assumed an effective charge separation, as obtained from the excited state calculations to be described below. We modeled the excited state by assuming the presence of a hole on the NO molecule. For that an electron was removed from the system. (This approximation for the excited state is only valid, if the electron and hole can be considered effectively separated. In our case, the electron was assumed to be delocalized in the CB of the substrate and thus spatially separated from the hole on the molecule.) We have confirmed the localization of the hole on the molecule (by calculating the difference of the charge density of the charged and neutral system), despite of the tendency of the PBE functional to delocalise states. Note, that the computation of a periodic system with a net charge usually requires the application of a charge correction

like the Freysoldt, Neugebauer and Van de Walle [20] method to exclude interactions of the charge with its periodic images. However, as we are not concerned with energetics of the charged state and additionally, the contributions of the initial charged and final (relaxed) geometry, for which a charge correction would be required, cancel each other out, a charge correction scheme is neglected.

For a later reference in the validation of the density functional tight binding (DFTB) [21] results, we computed the density of states (DOS) and projected DOS (PDOS) for the co-adsorption geometries. For this, a  $4 \times 4 \times 1$  BZ sampling and a convergence criterion of  $10^{-8}$  for the self consistent charge was used, to allow for improved accuracy of the DOS. Results were analyzed with the help of the vaspkit tool by Wang et al. [22]. To investigate the CT mechanism, we resorted to the DFTB method as implemented in the dftb+ code [23]. DFTB is an approximative density functional theory (DFT) method, where the total energy is expanded with respect to the charge fluctuations around a reference density. The repulsive energies for the nuclei are represented by pair interaction potentials. Using a suitable set of rigorously generated parameters, DFTB allows for accurate results at 2 to 3 order of magnitude faster computational times compared to DFT methods using local or semi-local approximations. Its time-dependent extension (TD-DFTB) allows us to compute excited state properties of large systems. A publicly available parameter set to describe titania is the *tiorg* set [24], which in combination with the *mio* set [25] for molecules, provides all parameters needed to model our systems. As we found discrepancies in the description of geometries and adsorption energies with respect to PBE results, we applied two modifications to these sets. First, we modified the N-Ti repulsive potential by fitting it to the PBE results for the NO molecule at different distances over a five-fold coordinated Ti atom on the (001) anatase surface (with the nitrogen atom of NO pointing towards the surface Ti). Second, we reduced the cut-off distance of the N-O repulsive potential of the *mio* set to 3.5 au, to correctly obtain the adsorption energy of NO onto a surface oxygen (forming

NO<sub>2</sub>). In the description of water, we used a hydrogen damping function [26] with a damping parameter of  $\eta = 4.05$ . This damping applies an empirical energy correction for the short range interactions with hydrogen atoms, improving on the description of hydrogen bonds. With these parameter modifications the PBE (co-)adsorption geometries and energies were reproduced.

TD-DFTB contains two implementations to obtain excited state properties. Firstly, TD-DFTB in the frequency domain [27–29], which describes the response of a system to a perturbation within the linear response regime. Secondly, a real-time implementation [30], which allows for the propagation of electronic states in the time domain. In the following we refer to the two implementations as LR-DFTB (linear response-DFTB) and RT-DFTB (real time DFTB), respectively. Both methods complement each other, since on the one hand the LR-DFTB methods allows the analysis of computed absorption spectra with respect to the states contributing to an excitation, on the other hand the RT-DFTB method enables the observation of electron dynamics with a time dependent external perturbation. In order to utilize their synergies we applied both methods. As LR-DFTB is currently implemented only for non-periodic systems, we have developed a cluster model to mimic the adsorption configurations found in the periodic models. We have cut out a cluster from a DFTB-relaxed pristine (001) surface slab. Cuts were made so that all sides were terminated by peripheral oxygens. The cluster structure consists of 3 TiO<sub>2</sub> layers. The peripheral oxygens were saturated with pseudo hydrogen atoms, in the following represented by H', in total constituting a structure of Ti<sub>37</sub>O<sub>104</sub>H'<sub>86</sub>. The H' were placed along the direction of the Ti-O bond, which the H'-O replaced, and the atomic numbers were chosen to maintain charge neutrality e.g., the atomic numbers and the H' positioning were computationally optimized for each layer to obtain an adequate fit of the homo-lumo gap to the bulk band gap. H'-O<sub>periph</sub> groups were kept fixed at the optimized positions, obtained from the gap fit, for all following DFTB calculations. Geometries for the adsorption of NO and H<sub>2</sub>O on the cluster surface were

optimized using DFTB. To assess the validity of our cluster model, we compared the DFTB density of states for the cluster (c-DOS) with the DOS obtained for the aforementioned super cell using periodic boundary conditions. Overall, the c-DOS compares well to the DOS for the periodic structure (for details see the supporting information (SI)). The obtained cluster structures are displayed in Fig. 1 (c) and (f).

Spin-unrestricted LR-DFTB calculations were then carried out on these structures. The first 400 excitations were calculated, which cover an energy range of up to  $\sim 3.5$  eV. The parameter energy window“, which defines the energy range above the last transition (defined by the number of excitations) to be included in the spectral calculation, was chosen as 0.1 H, to ensure sufficient convergence of the spectra while keeping the computational effort feasible. RT-DFTB spectra were obtained and compared to those obtained with the LR-DFTB method. RT-DFTB electron dynamics has been carried out for 200 fs, exciting the systems with a continuous laser pulse at different excitation energies, which were obtained from the absorption spectra of the systems. For that, the energies, which showed high peaks in the absorption spectrum, were chosen as 1.6 eV, 1.78 eV and 2.37 eV for the  $\text{NO}_{\text{OH}}$  system and 2.43 eV as well as 2.81 eV for the  $\text{NO}_{\text{Ti}}$  configuration.

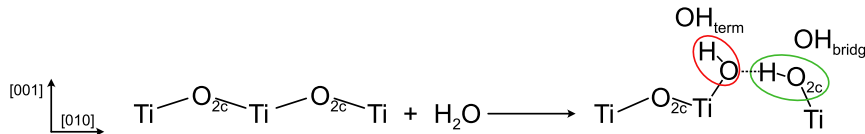
## Results

### Reaction pathways for the degradation of NO under visible light

Based on the results reported in Ref. [6] and the study of the  $\text{NO}_{\text{OH}}$  and  $\text{NO}_{\text{Ti}}$  co-adsorption geometries as displayed in Fig. 1, we propose two reaction pathways for the visible light assisted oxidation of NO. Both reaction pathways assume a CT excitation, where an electron is excited from NO to the  $\text{TiO}_2$  CB.

For clarity, we introduce a naming convention for the hydroxyl groups created via the dissociation of water on the surface, the bridging OH ( $\text{OH}_{\text{bridg}}$ ) and the terminal OH ( $\text{OH}_{\text{term}}$ ), which are graphically displayed in S. 1. Additionally to the naming convention,  $\dots$  shall

indicate a hydrogen bond and a dashed line  $--$  a weak electro static interaction.

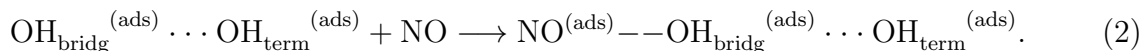


Scheme 1: Graphical representation of the water dissociation on the (001) anatase surface. A fracturing of a Ti-O bond with a two-fold coordinated oxygen ( $O_{2c}$ ) and its hydrogenation by a water molecule leads to the formation of two hydroxyl groups. These are bound on neighboring Ti atoms forming a bridging hydrogen bond. The two types of hydroxyl groups are named as bridging OH ( $OH_{bridg}$ ) and terminal OH ( $OH_{term}$ ).

When water dissociates on the anatase (001) surface, it spontaneously splits into an OH group, which adsorbs on a Ti binding site, and a hydron, which hydroximates a surface oxygen. This results in the formation of two hydroxyl groups, a bridging  $OH_{bridg}$  and a terminal  $OH_{term}$ , which interact via a hydrogen bond.



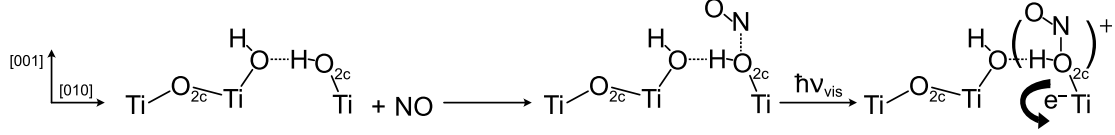
From this, the adsorption of NO on the bridging OH group is given by



This adsorption configuration shall be denoted as  $HONO_i$  in the following. Note, that the adsorption of NO on a neighboring Ti binding site is energetically favored over this adsorption geometry. That is why, the  $HONO_i$  is only found to be stable, when the the neighboring Ti binding site is saturated with hydroxyl groups.

When the system is excited with visible light, we obtain





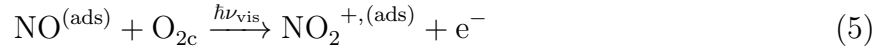
Scheme 2: Schematic model of the reaction pathway to form HONO starting from a dissociated water model. The NO molecule adsorbs weakly on the bridging hydroxyl group. After the excitation with visible light NO forms a chemical bond with the  $\text{OH}_{\text{bridg}}$  group, yielding a positively charged HONO molecule.

This final configuration shall hereafter be named  $\text{HONO}_f$ . The two reactions are additionally schematically displayed in the S. 1 (water dissociation) and S. 2 (HONO formation), displaying also geometric configurations.

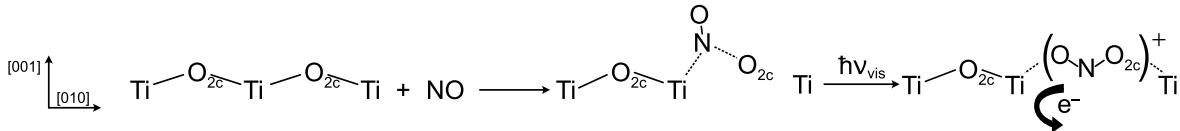
The second suggested reaction starts from the adsorption of NO on a Ti binding site, which was found to be the most stable adsorption configuration for NO on the anatase (001) surface.



Given this initial configuration, in the following called  $\text{NO}_i$ , an excitation with visible light leads to the formation of a  $\text{NO}_2^+$  molecule with a two fold coordinated surface oxygen  $\text{O}_{2c}$ .



This final configuration shall hereafter be denoted by  $\text{NO}_f$ . The graphical representation of this reaction can be found in S. 3.



Scheme 3: Reaction pathway representation for the formation of an  $\text{NO}_2$  ion by the adsorption of NO on a two fold coordinated surface oxygen after the excitation with visible light.

## Nudged Elastic Band calculations

In order to ensure, that the ahead discussed reactions do not occur spontaneously without excitation, we performed NEB calculations. The NEB images were chosen in accordance to the reaction equations as  $\text{NO}_i$  and  $\text{HONO}_i$  for the initial images and a stable neutral system in the final configuration, which best resembled the  $\text{NO}_f$  and  $\text{HONO}_f$ . For  $\text{NO}_f$  we found a stable final configuration in the ground state (GS) (which is  $\sim 0.2$  eV more stable than the  $\text{NO}_i$ ). The HONO molecule was only found to be stable in the vacuum. In order to create this structure the  $\text{OH}_{\text{bridg}}$  and the NO were removed from the surface, while enforcing a bond creation between the nitrogen and oxygen of the OH group. The  $\text{OH}_{\text{term}}$  remained on the surface.

The evaluated reaction barriers are displayed in Fig. 2, with a graphical representation of the initial (black), final (cyan) and transition state (green). While the formation of HONO in vacuum constitutes an energy barrier of 1.29eV and is significantly too high, to occur spontaneously in the GS, the reaction barrier to form  $\text{NO}_2$  lies by solely 0.11 eV. Despite the relatively small energy barrier, a reaction will not occur spontaneously at room temperature, because vibrations or rotations, which could mediate such a reaction, possess energies of around  $\sim 0.025$  eV (calculated as a rough estimate from a canonical ensemble). Considering these results we can state, that the suggested reactions do not occur without excitation.

## Density of States and Absorption Spectra

The DOS for both initial structures ( $\text{NO}_i$  and  $\text{HONO}_i$ ) was computed at the DFT and DFTB level of theory. Results can be found in figure (3). We can observe NO states in the gap region for all adsorption structures and levels of theory.

For the  $\text{HONO}_i$  geometry, the occupied  $\pi^*$  orbital is positioned just below the CB edge. All unoccupied orbitals mix with the  $\text{TiO}_2$  CB. This positioning compares well between PBE and DFTB results, despite the fact, that the band gap is larger for DFTB. The larger gap

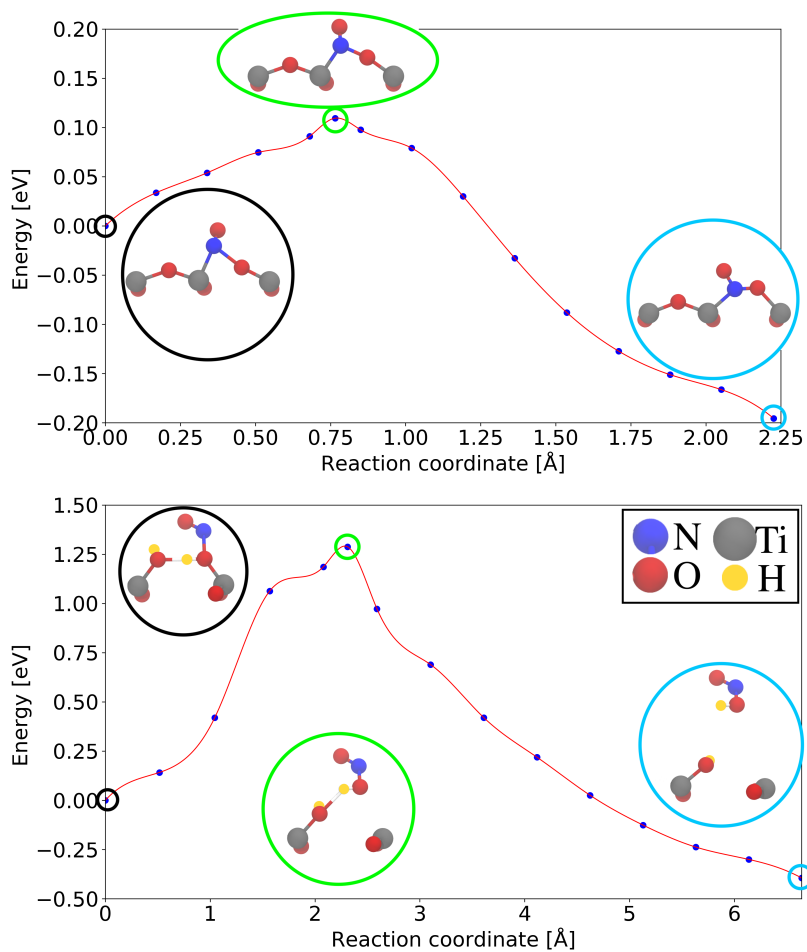


Figure 2: NEB reaction barriers for the reactions of NO to NO<sub>O<sub>2c</sub></sub> (top) and NO to HONO (bottom). The structural images in the picture give the initial, transition state and final geometries for the NEBs. Reaction barriers are 0.11 eV and 1.29 eV per NO molecule for NO<sub>O<sub>2c</sub></sub> and HONO, respectively.

of DFTB lies with its 2.9 eV close to experimentally observed band gaps for anatase with  $\sim 3.15$  eV. States related to OH groups lie deep in the VB and the CB.

The DOS for an adsorbed NO is similar to that of HONO, solely the positioning of NO pDOS is shifted to lower energies compared to its HONO counterpart. This leads to a shift of an unoccupied  $\pi^*$  orbital in the gap region for the DFTB results. PBE does not show this behaviour. Overall the DOS of DFTB and PBE compare well.

The spectra obtained from LR-DFTB calculations are illustrated in Fig. (4). All spectra show a ligand to metal oxide (L2M) CT excitation for energies in below 2.7 eV, which corresponds to excitations from the occupied NO orbital to  $\text{TiO}_2$  CB states. The  $\text{HONO}_i$  spectra show 3 main peaks at  $1.6\text{eV}$ ,  $1.78\text{eV}$  and  $2.37\text{eV}$ , for which the molar extinction coefficient  $\epsilon$  shows a maximum. The  $\text{NO}_i$  spectrum shows two neighboring maxima peaks at  $2.43\text{eV}$  and  $2.81\text{eV}$ . The spectrum of  $\text{NO}_i$  also depicts metal oxide to ligand (M2L) CT excitations, corresponding to an excitation of electrons from the  $\text{TiO}_2$  VB to the unoccupied NO orbital(s). These excitations overlap with the L2M excitations, as the unoccupied spin down orbitals lies close in energy to the occupied one. This results in a competition of a M2L and L2M CT excitation, which is in accordance to the findings of Ref. [6]. Quantitative differences to the Reference result in the different repulsives and cluster structures used.

B2B transitions are illustrated in orange and for the graph of  $\text{HONO}_i$  contain M2L transitions, as the unoccupied NO states lie within the CB. The M2L transitions are thus not illustrated for those states directly.

## RT-DFTB and Charged DFT

All peaks marked with an arrow were excited in a real time TD-DFTB calculation using a laser at the energies while freezing the ion dynamics. The electron dynamics were observed as depicted for a selected example in Fig. (5) and (6). All images of Fig. (5) show a CT

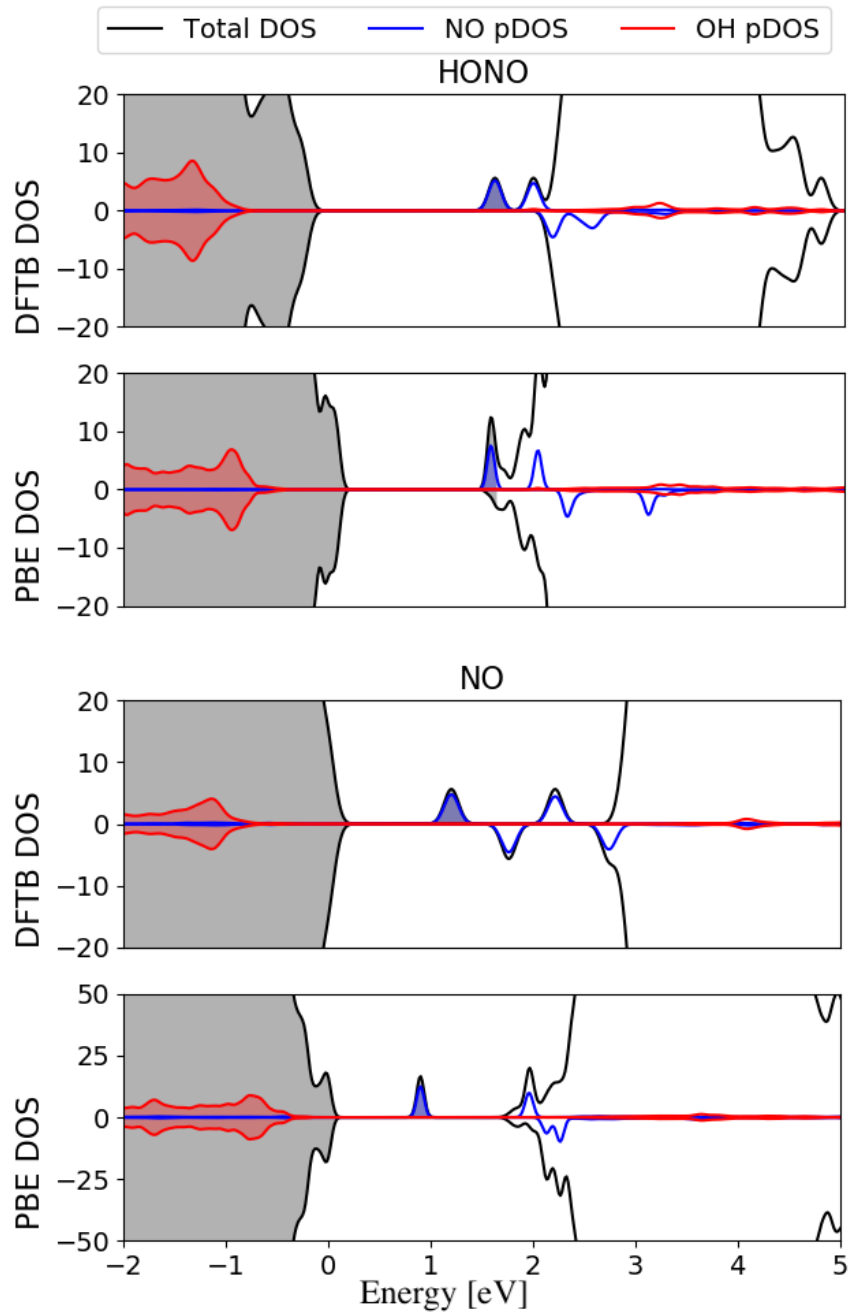


Figure 3: DFTB-c to PBE comparison of the density of states in arbitrary units for HONO (top) and NO (bottom). The spin up and spin down contributions are displayed with a positive and a negative DOS, respectively. The black line indicates the DOS of the total system, while red indicates the pDOS of the adsorbed OH groups, the NO pDOS is displayed in blue. Occupied states are indicated by filled areas under the curve.

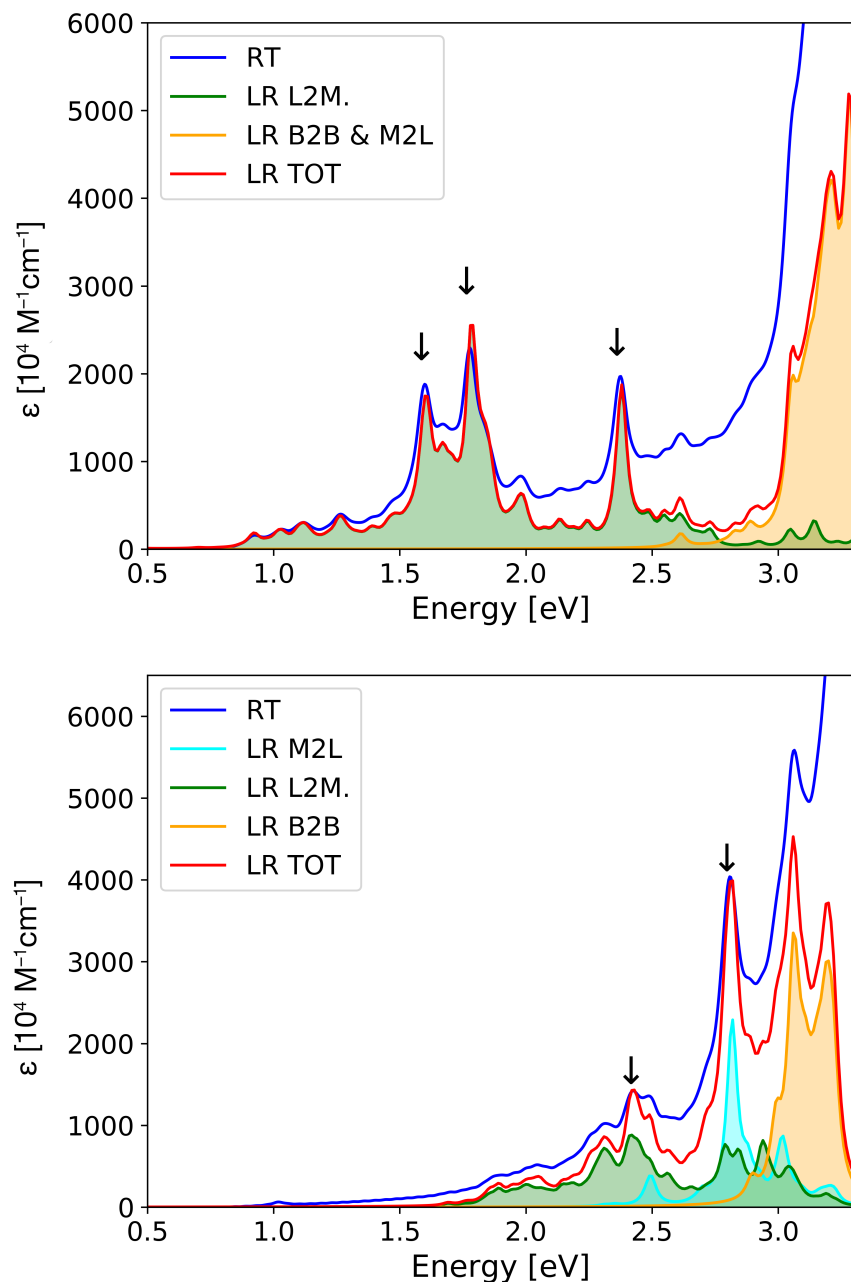


Figure 4: Spectra for HONO (top) and NO (bottom) obtained from Linear Response (LR) and Real-Time (RT) DFTB calculations. Ligand to metal oxide (L2M) CT excitations are denoted in green, band to band transitions are denoted in orange. Metal oxide to ligand (M2L) excitations lie within the B2B transitions and are solely displayed for the example of NO in cyan. Results for the RT spectra were multiplied by a factor of 650 for the HONO structure and 470 for NO to match the LR results.

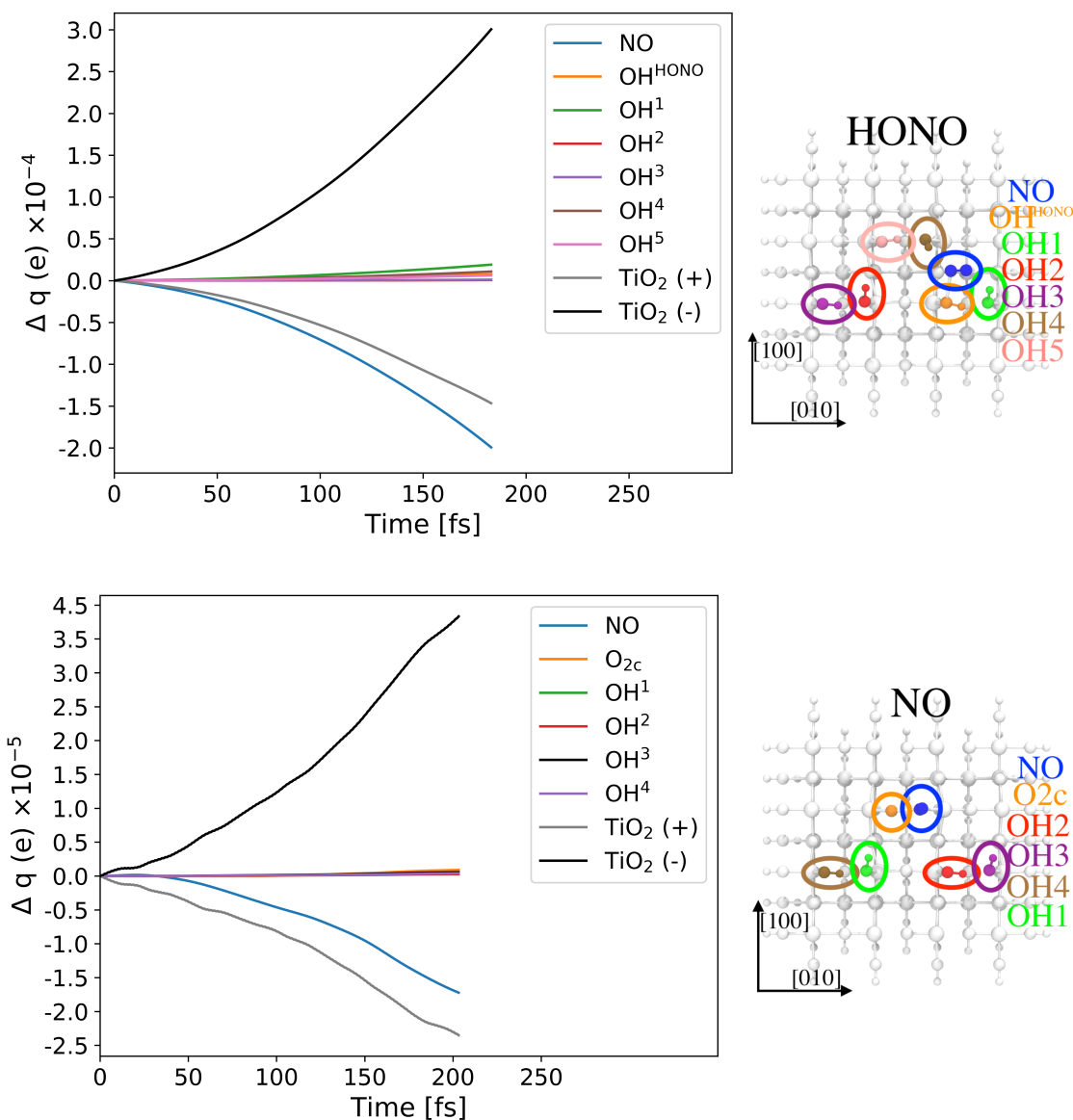


Figure 5: Electron dynamics results for HONO (top) and NO (bottom) are displayed for excitation energies of 1.6eV and 2.45eV, respectively. The graphics on the right give information on the geometrical arrangements of adsorbents in the top view on the cluster structures, following the naming convention used for the charges. Charges in the left graphics are given as Mulliken charges and were averaged over the time interval of 200fs to exclude high-frequency oscillations. Small contributions of atoms on TiO<sub>2</sub> are summed up for the negative and positive charge separately to show a possible charge separation also within the metal oxide.

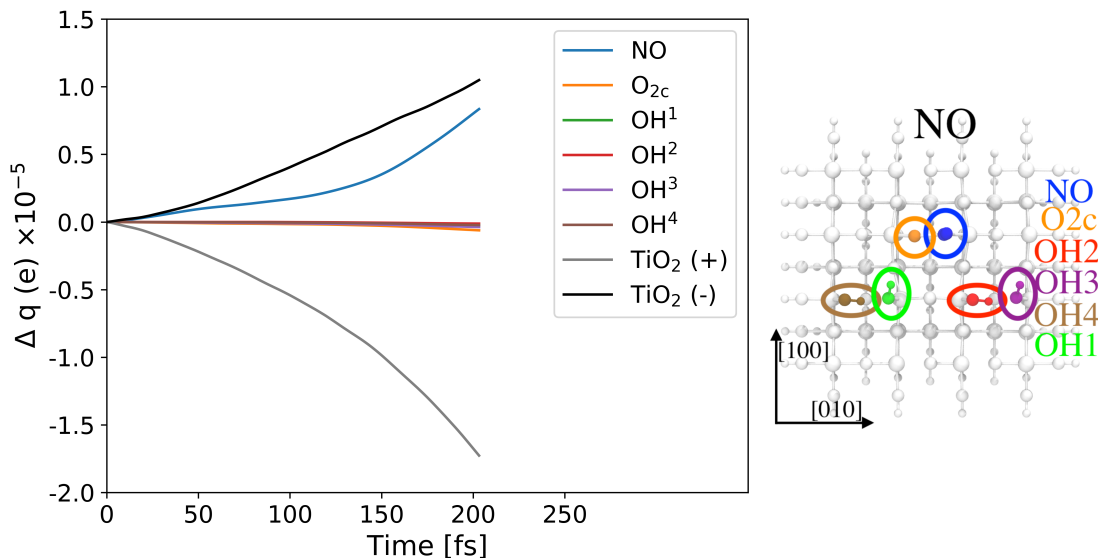


Figure 6: Electron dynamics results for NO are displayed for an excitation energy of 2.81 eV. Charges are given as Mulliken charges and were averaged over the time interval of 200fs to exclude high-frequency oscillations. Small contributions of atoms on  $TiO_2$  are summed up for the negative and positive charge separately to show a possible charge separation also within the metal oxide. The right image shows the geometrical arrangement of the adsorbents in top view with the naming conventions as used for the charge dynamics graph.

from the NO molecule to titania. Further analysis of the relevant wave functions for this CT show, that the charge is transferred from a localized NO  $\pi^*$  orbital to over the titania structure delocalized orbitals, which belong to the  $TiO_2$  CB. The OH groups from the water dissociated on the surface are not charged over the entire simulation time of 200fs. These observations are showing in accordance to the analysis of the spectra, that NO has formed in both the  $NO_i$  and the  $HONO_i$  configurations a CT complex, allowing for a L2M CT. Note, that the HONO configuration leads to a CT, that is an order of magnitude higher than that of the NO counter part, which might either arise from limitations of the TD-DFTB method or indicate a stronger CT complexation with the substrate (over the  $OH_{bridg}$  group).

The charge dynamics for excitation energies, which are not displayed here, do show qualitatively the same behavior as the ones displayed in the example images. Solely the excitation of the NO molecule at 2.81 eV represents an exception from the ahead discussed CT mech-

anism. The excitation at 2.81 eV results in an inversion of the CT direction, resulting in a CT from titania to the NO molecule, charging it negatively, as displayed in Fig (6). This is in accordance to the observation of Ref. [6], which predicted a competing L2M and M2L CT mechanism depending on the excitation energy, with a preference for the L2M CT at lower energies.

Note, that the observed different charges of  $\text{TiO}_2$  for the cases of HONO and NO depict an overall uniform reduction of the Ti-O bond polarization, e.g. the Ti charge negatively and the O charge positively in very small contributions. The different charges in the cases considered do not show an electron hole pair formation resulting in a local charge separation within the cluster. This allows the conclusion, that on average the metal oxide charges negatively for the cases illustrated in Fig. (5) and positively for the case illustrated in Fig. (6). The ahead discussed CT behaviour indicates a charge separation between the positive charge on the NO molecule, and the negative charge in the  $\text{TiO}_2$  CB for most excitation energies in the visible (except for the competing mechanism of a M2L CT for the NO structure. As for most energies in the visible the L2M CT is predicted to be dominant we omit this case for the following evaluation of reactions). This predicted behaviour allows us to model the excited state by performing a charged PBE calculation with a positive charge localized on the NO molecule.

The charged calculations, showed for the case of the HONO geometry a spontaneous bond formation between the NO and the bridging OH, resulting in the formation of an adsorbed HONO molecule (from an adsorption distance of  $2.41\text{\AA}$  the bond lengths in the charged state yielded  $1.62\text{\AA}$ , see Fig. 7 (left)). For the case of NO adsorbed on a Ti adsorption site, the NO turns to form a bond with the neighboring surface oxygen, resulting in the formation of an adsorbed  $\text{NO}_2^+$  molecule in a geometry similar to the one observed in the GS (from  $2.02\text{\AA}$  the bond length reduces to  $1.38\text{\AA}$ , see Fig. 7 (right)).

Thus, we could show a reaction of NO with adsorbed hydroxyl groups as well as a  $\text{NO}_2$  formation with a surface oxygen are possible to occur as a result of a CT excitation under

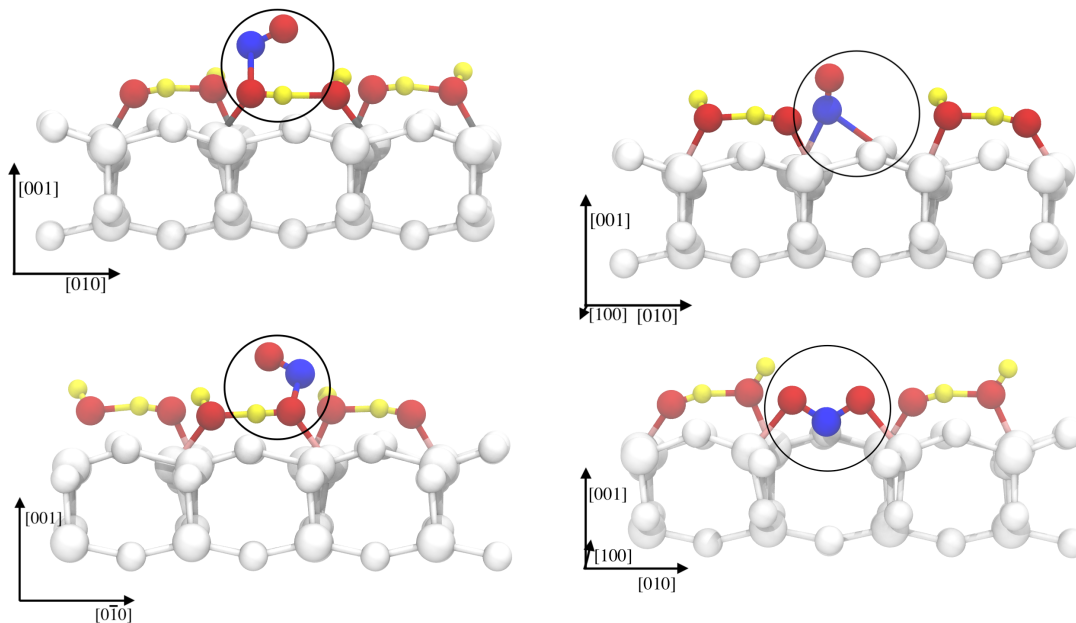


Figure 7: Relaxed geometries in the positive charged state for HONO (left bottom) and  $\text{NO}_2$  (right bottom). Note the differences in the bond formation compared to the initial neutral configurations given in in top (left HONO and right NO).

visible light. A continued reaction with  $\text{OH}^-$  groups as present in water, will be possible for the charged molecules.

## Conclusions

*Freitag et al.* [6] observed experimentally that the pollutant nitric oxide (NO) does degrade on anatase  $\text{TiO}_2$  upon illumination with visible light. Under the presence of water NO then forms nitric acid ( $\text{HNO}_3$ ) as well as by-products, i.e.  $\text{NO}_2$ ,  $\text{HNO}_2$ .

While it is well known, that NO degrades on anatase under the illumination with UV light, a reaction induced by excitation in the visible region of the spectrum has been little studied so far. In order to explain the visible light activity, Ref. [6] suggested a reaction based on a CT complexation of the NO molecule and the substrate. However, this conclusion was made on the grounds of TD-DFTB evaluations of NO- $\text{TiO}_2$  complexes excluding the role of water, despite the claim of the authors of  $\text{H}_2\text{O}$ s main role in the reaction.

That is why, this work set out to investigate NO oxidation mechanisms and analyze the role of water therein. According to the proposal of a CT mechanism and on the grounds of PBE GS computations of NO-H<sub>2</sub>O co-adsorption geometries on the anatase (001) surface, we proposed two reactions mediated by a visible light induced CT process. These were subsequently confirmed by theoretical investigations in three steps. Firstly, the occurrence of a spontaneous reaction was excluded by means of NEB calculations. Secondly, TD-DFTB calculations showed the formation of a ligand to metal oxide (L2M) CT complex. Our results indicated, that an excitation in the visible does in most cases lead to the creation of a hole on the NO molecule and an electron in the CB of TiO<sub>2</sub>. Note, a few cases showed a metal oxide to ligand (M2L) CT, but the L2M is dominant for lower energies. Lastly, the excited state was modeled by PBE calculations with a positive charge located on NO. Based on these computations, it has been found that after excitation the NO<sup>+</sup> interacts with adsorbed OH groups to form HONO<sup>+</sup> or with a surface oxygen to form NO<sub>2</sub><sup>+</sup>. The latter reaction did not show influence of adsorbed water.

Overall two possible CT induced oxidation mechanisms for NO have been demonstrated, which showed the formation of HONO<sup>+</sup> by the interaction with water or the formation of NO<sub>2</sub><sup>+</sup> with a surface oxygen. For the latter no interaction with water was found.

## References

- [1] Eurostat. *Air pollution statistics - air emissions accounts*. [https://ec.europa.eu/eurostat/statistics-explained/index.php?title=Air\\_pollution\\_statistics\\_-\\_air\\_emissions\\_accounts](https://ec.europa.eu/eurostat/statistics-explained/index.php?title=Air_pollution_statistics_-_air_emissions_accounts). 2020.
- [2] Eurostat. *Air pollution statistics - emission inventories*. [https://ec.europa.eu/eurostat/statistics-explained/index.php?title=Air\\_pollution\\_statistics\\_-\\_emission\\_inventories&oldid=394947#General\\_overview](https://ec.europa.eu/eurostat/statistics-explained/index.php?title=Air_pollution_statistics_-_emission_inventories&oldid=394947#General_overview). 2020.

- [3] Janusz Lasek, Yi-Hui Yu, and Jeffrey C.S. Wu. “Removal of NO<sub>x</sub> by photocatalytic processes”. In: *Journal of Photochemistry and Photobiology C: Photochemistry Reviews* 14 (2013), pp. 29–52. ISSN: 1389-5567. DOI: <https://doi.org/10.1016/j.jphotochemrev.2012.08.002>. URL: <https://www.sciencedirect.com/science/article/pii/S1389556712000615>.
- [4] David C. Carslaw, Sean D. Beevers, and Margaret C. Bell. “Risks of exceeding the hourly EU limit value for nitrogen dioxide resulting from increased road transport emissions of primary nitrogen dioxide”. In: *Atmospheric Environment* 41.10 (2007), pp. 2073–2082. ISSN: 1352-2310. DOI: <https://doi.org/10.1016/j.atmosenv.2006.10.074>. URL: <https://www.sciencedirect.com/science/article/pii/S1352231006011058>.
- [5] Qingping Wu and Roel van de Krol. “Selective Photoreduction of Nitric Oxide to Nitrogen by Nanostructured TiO<sub>2</sub> Photocatalysts: Role of Oxygen Vacancies and Iron Dopant”. In: *J. Am. Chem. Soc.* 134 (2012), pp. 9369–9375.
- [6] J. Freitag et al. “Nitrogen(II) Oxide Charge Transfer Complexes on TiO<sub>2</sub>: A New Source for Visible-Light Activity”. In: *J. Phys. Chem. C* 119 (2015), pp. 4488–4501.
- [7] Dieqing Zhang et al. “Au nanoparticles enhanced rutile TiO<sub>2</sub> nanorod bundles with high visible-light photocatalytic performance for NO oxidation”. In: *Applied Catalysis B: Environmental* 147 (2014), pp. 610–616. ISSN: 0926-3373. DOI: <https://doi.org/10.1016/j.apcatb.2013.09.042>. URL: <https://www.sciencedirect.com/science/article/pii/S0926337313006073>.
- [8] Andrea Folli et al. “Role of TiO<sub>2</sub> surface hydration on NO oxidation photo-activity”. In: *Journal of Photochemistry and Photobiology A: Chemistry* 220.2 (2011), pp. 85–93. ISSN: 1010-6030. DOI: <https://doi.org/10.1016/j.jphotochem.2011.03.017>. URL: <https://www.sciencedirect.com/science/article/pii/S1010603011001225>.

- [9] Sid Devahasdin et al. “TiO<sub>2</sub> photocatalytic oxidation of nitric oxide: transient behavior and reaction kinetics”. In: *Journal of Photochemistry and Photobiology A: Chemistry* 156.1 (2003), pp. 161–170. ISSN: 1010-6030. DOI: [https://doi.org/10.1016/S1010-6030\(03\)00005-4](https://doi.org/10.1016/S1010-6030(03)00005-4). URL: <https://www.sciencedirect.com/science/article/pii/S1010603003000054>.
- [10] Henri Courbon and Pierre Pichat. “Room-temperature interaction of N<sub>2</sub>O with ultraviolet-illuminated titanium dioxide”. In: *J. Chem. Soc., Faraday Trans. 1* 80 (11 1984), pp. 3175–3185. DOI: 10.1039/F19848003175. URL: <http://dx.doi.org/10.1039/F19848003175>.
- [11] A. Domínguez García et al. “Extensions of the Time-Dependent Density Functional Based Tight-Binding Approach”. In: *J. Chem. Theory. Comput.* 9 (202013), pp. 4901–4914.
- [12] J. P. Perdew, K. Burke, and M. Ernzerhof. “Generalized Gradient Approximation Made Simple”. In: *Phys. Rev. Lett.* 77 (18 Oct. 1996), pp. 3865–3868. DOI: 10.1103/PhysRevLett.77.3865.
- [13] G. Kresse and J. Furthmüller. In: *Phys. Rev. B* 54 (1996), pp. 11169–11186.
- [14] G. Kresse and D. Joubert. In: *Phys. Rev.* 59 59 (1999), pp. 1758–1775.
- [15] H. J. Monkhorst and J. D. Pack. “Special points for Brillouin-zone integrations”. In: *Phys. Rev. B* 13 (1976), p. 5188.
- [16] Daniel Sheppard et al. “A generalized solid-state nudged elastic band method”. In: *The Journal of Chemical Physics* 136.7 (2012), p. 074103. DOI: 10.1063/1.3684549. eprint: <https://doi.org/10.1063/1.3684549>. URL: <https://doi.org/10.1063/1.3684549>.
- [17] Graeme Henkelman, Blas P. Uberuaga, and Hannes Jónsson. “A climbing image nudged elastic band method for finding saddle points and minimum energy paths”. In: *The Journal of Chemical Physics* 113.22 (2000), pp. 9901–9904. DOI: 10.1063/1.1329672.

- eprint: <https://doi.org/10.1063/1.1329672>. URL: <https://doi.org/10.1063/1.1329672>.
- [18] Graeme Henkelman and Hannes Jónsson. “A dimer method for finding saddle points on high dimensional potential surfaces using only first derivatives”. In: *The Journal of Chemical Physics* 111.15 (1999), pp. 7010–7022. DOI: 10.1063/1.480097. eprint: <https://doi.org/10.1063/1.480097>. URL: <https://doi.org/10.1063/1.480097>.
- [19] Penghao Xiao et al. “Solid-state dimer method for calculating solid-solid phase transitions”. In: *The Journal of Chemical Physics* 140.17 (2014), p. 174104. DOI: 10.1063/1.4873437. eprint: <https://doi.org/10.1063/1.4873437>. URL: <https://doi.org/10.1063/1.4873437>.
- [20] C. Freysoldt, J. Neugebauer, and C. G. Van de Walle. “Fully Ab Initio Finite-Size Corrections for Charged-Defect Supercell Calculations”. In: *Physical Review Letters* 102 (2009), p. 016402. URL: <https://doi.org/10.1103/PhysRevLett.102.016402>.
- [21] B. Aradi, B. Hourahine, and T. Frauenheim. “DFTB+, a Sparse Matrix-Based Implementation of the DFTB Method”. In: *J. Phys. Chem. A* 111 (2007), p. 5678.
- [22] Jin-Cheng Liu Ve Wang Nan Xu. “VASPKIT: A Pre- and Post-Processing Program for the VASP Code.” In: 2014. URL: <http://vaspkit.sourceforge.net>.
- [23] B. Hourahine et al. “DFTB+, a software package for efficient approximate density functional theory based atomistic simulations”. In: *The Journal of Chemical Physics* 152.12 (2020), p. 124101. DOI: 10.1063/1.5143190. eprint: <https://doi.org/10.1063/1.5143190>. URL: <https://doi.org/10.1063/1.5143190>.
- [24] Grygoriy Dolgonos et al. “An Improved Self-Consistent-Charge Density-Functional Tight-Binding (SCC-DFTB) Set of Parameters for Simulation of Bulk and Molecular Systems Involving Titanium”. In: *J. Chem. Theory. Comput.* 6 (2010), pp. 266–278.

- [25] M. Elstner et al. “Self-consistent-charge density-functional tight-binding method for simulations of complex materials properties”. In: *Phys. Rev. B* 58 (11 Sept. 1998), pp. 7260–7268. DOI: 10.1103/PhysRevB.58.7260. URL: <https://link.aps.org/doi/10.1103/PhysRevB.58.7260>.
- [26] Michael Gaus, Qiang Cui, and Marcus Elstner. “DFTB3: Extension of the Self-Consistent-Charge Density-Functional Tight-Binding Method (SCC-DFTB)”. In: *Journal of Chemical Theory and Computation* 7.4 (2011), pp. 931–948. DOI: 10.1021/ct100684s. eprint: <https://doi.org/10.1021/ct100684s>. URL: <https://doi.org/10.1021/ct100684s>.
- [27] M. E. Casida. *Recent Advances in Density Functional Methods, Part I*. World Scientific, 1995. Chap. Chapter: Time-Dependent Density-Functional Response Theory for Molecules, pp. 155–192.
- [28] A. Domínguez et al. “Extensions of the Time-Dependent Density Functional Based Tight-Binding Approach”. In: *Journal of Chemical Theory and Computation* 9.11 (2013). PMID: 26583409, pp. 4901–4914. DOI: 10.1021/ct400123t. eprint: <https://doi.org/10.1021/ct400123t>. URL: <https://doi.org/10.1021/ct400123t>.
- [29] T. A. Niehaus et al. “Tight-binding approach to time-dependent density-functional response theory”. In: *Phys. Rev. B* 63 (8 Feb. 2001), p. 085108. DOI: 10.1103/PhysRevB.63.085108. URL: <https://link.aps.org/doi/10.1103/PhysRevB.63.085108>.
- [30] F. Bonafé et al. “A Real-Time Time-Dependent Density Functional Tight-Binding Implementation for Semiclassical Excited State Electron-Nuclear Dynamics and Pump-Probe Spectroscopy Simulations”. In: *J. Chem. Theory. Comput.* 16 (2020), pp. 4454–4469.